

The fraction of strongly bound cross-bridges is increased in mice that carry the myopathy-linked myosin heavy chain mutation MYH4^{L342Q}

Johan Lindqvist^{1,*}, Hiroyuki Iwamoto², Gonzalo Blanco³ and Julien Ochala^{1,4}

SUMMARY

Myosinopathies have emerged as a new group of diseases and are caused by mutations in genes encoding myosin heavy chain (MyHC) isoforms. One major hallmark of these diseases is skeletal muscle weakness or paralysis, but the underlying molecular mechanisms remain unclear. Here, we have undertaken a detailed functional study of muscle fibers from *Myh4^{arl}* mice, which carry a mutation that provokes an L342Q change within the catalytic domain of the type IIb skeletal muscle myosin protein MYH4. Because homozygous animals develop rapid muscle-structure disruption and lower-limb paralysis, they must be killed by postnatal day 13, so all experiments were performed using skeletal muscles from adult heterozygous animals (*Myh4^{arl}/+*). *Myh4^{arl}/+* mice contain MYH4^{L342Q} expressed at 7% of the levels of the wild-type (WT) protein, and are overtly and histologically normal. However, mechanical and X-ray diffraction pattern analyses of single membrane-permeabilized fibers revealed, upon maximal Ca²⁺ activation, higher stiffness as well as altered meridional and equatorial reflections in *Myh4^{arl}/+* mice when compared with age-matched WT animals. Under rigor conditions, by contrast, no difference was observed between *Myh4^{arl}/+* and WT mice. Altogether, these findings prove that, in adult MYH4^{L342Q} heterozygous mice, the transition from weak to strong myosin cross-bridge binding is facilitated, increasing the number of strongly attached myosin heads, thus enhancing force production. These changes are predictably exacerbated in the type IIb fibers of homozygous mice, in which the embryonic myosin isoform is fully replaced by MYH4^{L342Q}, leading to a hypercontraction, muscle-structure disruption and lower-limb paralysis. Overall, these findings provide important insights into the molecular pathogenesis of skeletal myosinopathies.

INTRODUCTION

Myosinopathies are a group of heterogeneous myopathies with wide clinical variability, including different grades of severity and ages of onset (congenital, childhood or adulthood) (Oldfors, 2007). They are often associated with skeletal muscle weakness or paralysis and are caused by mutations in genes encoding myosin heavy chain (MyHC) isoforms that are present in mammalian muscle in the fetus, newborn and/or adult [e.g. MYH3, MYH8, MYH7, MYH2 and MYH4 (encoding embryonic, perinatal, type I, type IIa and type IIb MyHC isoforms, respectively)] (Kurapati et al., 2012; Oldfors, 2007). To date, only a few of these mutations have been functionally characterized, preventing an in-depth molecular understanding of the weakness or paralysis in myosinopathies (Belus et al., 2008; Debold et al., 2007; Keller et al., 2004; Palmiter et al., 2000; Seeböhm et al., 2009; Wang et al., 2003).

Mutations in genes encoding MyHCs are typically missense, resulting in the substitution of just one amino acid, and have been identified within the catalytic domain, converter and rod (backbone)

regions of the myosin molecule (Rayment et al., 1995). The ones in the catalytic domain are of particular interest because this region is essential for actomyosin interaction, force production and motion. Indeed, it has (i) specific binding sites where phosphate (Pi), ATP and adenosine diphosphate (ADP) can be exchanged; and (ii) various actin-binding locations (Rayment et al., 1993a; Rayment et al., 1993b; Rayment et al., 1996). Recently, a mouse model expressing a particular MYH4 mutation, MYH4^{L342Q}, in the catalytic domain of type IIb MyHC (MyHC IIb) was characterized (Kurapati et al., 2012). Homozygous mice (*Myh4^{arl}/Myh4^{arl}*) are indistinguishable from wild-type (WT) animals from birth to postnatal day 11. Nevertheless, from day 11, coinciding with the timing of replacement of neonatal and embryonic MyHC isoforms by the adult types, a sudden skeletal muscle degeneration process occurs as attested by the absence of structured thick filaments and accumulation of intracellular protein aggregates, leading to hind-limb paralysis by day 13 (Kurapati et al., 2012). The speed and severity of the myopathic phenotype in homozygous mice makes it difficult to use them to obtain insights into the molecular functional consequences of the MYH4^{L342Q} myosin mutation. Heterozygous mice (*Myh4^{arl}/+*) are, by contrast, a convenient source of material because they do not suffer from any overt pathological or morphological change in the muscles (Fig. 1) and have a normal lifespan. Crucially, quantitative proteomic analysis of the MyHC IIb content in the muscles of heterozygous mice has shown that MYH4^{L342Q} is present at 7% of the WT protein levels (Kurapati et al., 2012). Interestingly, single membrane-permeabilized muscle fibers isolated from adult *Myh4^{arl}/+* animals have been shown to produce higher steady-state isometric maximal forces than those from WT (Fig. 1) (Kurapati et al., 2012). Thus,

¹Department of Neuroscience, Uppsala University, Uppsala 751 85, Sweden

²Japan Synchrotron Radiation Research Institute, SPring-8, Hyogo 679-5198, Japan

³Biology Department, University of York, York, YO10 5DD, UK

⁴Centre of Human and Aerospace Physiological Sciences, School of Biomedical Sciences, King's College London, London, SE3 8TL, UK

*Author for correspondence (johan.lindqvist@neuro.uu.se)

Received 15 October 2012; Accepted 10 January 2013

© 2013. Published by The Company of Biologists Ltd
This is an Open Access article distributed under the terms of the Creative Commons Attribution Non-Commercial Share Alike License (<http://creativecommons.org/licenses/by-nc-sa/3.0/>), which permits unrestricted non-commercial use, distribution and reproduction in any medium provided that the original work is properly cited and all further distributions of the work or adaptation are subject to the same Creative Commons License terms.

TRANSLATIONAL IMPACT

Clinical issue

Myosinopathies, which are caused by mutations in genes encoding myosin heavy chain (MyHC) isoforms, are an emerging group of inherited diseases that are characterized by skeletal muscle weakness, paralysis and degeneration. These diseases show wide clinical variability and, to date, the underlying mechanisms of paralysis are poorly understood. Recently, a mouse mutant expressing a particular mutation (*Myh4^{ar1}*) affecting myosin function was characterized. However, mice that are homozygous for this mutation are difficult to use to gain mechanistic insights into myosinopathies because of the speed and severity of muscular degeneration.

Results

In this work, the authors performed an in-depth functional study of muscle fibers in a unique mouse model that exhibits lower-limb paralysis and closely mimics human myosinopathies. To overcome problems encountered when working with *Myh4^{ar1}* homozygous mice, the authors studied heterozygous mice. By comparing the mechanics and X-ray diffraction patterns of mutated and wild-type muscle fibers, the authors provide evidence that the myosin mutation enhances the amount of strongly bound myosin cross-bridges and facilitates force production at the molecular and cellular level. These findings suggest a mechanism for the occurrence of hypercontraction, muscle-structure disruption and lower-limb paralysis in affected mice.

Implications and future directions

This study unveils for the first time the cascade of events leading to contractile deregulation in the presence of a myosin mutation. Thus, the work provides important insights into the molecular and cellular pathogenesis of myosinopathies. In light of these findings, future potential therapies should focus on restoring myosin function to reverse muscle paralysis.

one can hypothesize that, in the presence of MYH4^{L342Q}, the formation of strongly bound myosin cross-bridges is increased and this might be the molecular determinant of muscle-structure disruption and paralysis in *Myh4^{ar1}/Myh4^{ar1}* mice. In the present study, we aimed to test this by recording and analyzing the mechanics and X-ray diffraction patterns of muscle fibers from adult *Myh4^{ar1}/+* and control mice.

RESULTS

Single membrane-permeabilized fiber mechanics

The MyHC isoform distribution was not different between *Myh4^{ar1}/+* and WT mice (Fig. 2). Nevertheless, here, comparisons were restricted to cells expressing MyHC IIb. As previously shown (Kurapati et al., 2012), steady-state isometric force at saturating Ca²⁺ concentration ($[Ca^{2+}]$ $[-\log_{10} [Ca^{2+}]$ (pCa) 4.50] was significantly higher in *Myh4^{ar1}/+* when compared with WT mice (Fig. 1). To analyze the behavior at non-saturating $[Ca^{2+}]$ (pCa 6.30–4.90), the relative force-pCa relationship was constructed (Fig. 2) and fitted using the following sigmoid Hill equation: $F = [Ca^{2+}]^{nH} / ([Ca_{50}]^{nH} + [Ca^{2+}]^{nH})$, where F is force; $-\log_{10} [Ca_{50}]$ is the midpoint (pCa₅₀ or Ca²⁺ sensitivity); and nH is the Hill coefficient. pCa₅₀ was significantly higher in *Myh4^{ar1}/+* when compared with WT mice (Fig. 2). To obtain some information regarding the mechanisms underlying the force enhancement with MYH4^{L342Q}, stiffness measurements were performed. Thus, step changes in fiber length were imposed (releases of 0.15, 0.3 and 0.5% of fiber length and stretches of the same amplitudes). Stiffness was defined as the slope of the linear regression of the relationship between the peak force response and the length change (Fig. 3). Active stiffness was

significantly higher at saturating $[Ca^{2+}]$ (pCa 4.50) in *Myh4^{ar1}/+* when compared with WT mice (Table 1). By contrast, under rigor conditions, where all myosin heads are attached owing to a very slow dissociation rate (Cooke and Franks, 1980), rigor stiffness was not different between *Myh4^{ar1}/+* and WT mice (Table 1).

X-ray diffraction patterns

To gain further insights into the changes with the MYH4^{L342Q} mutation, low-angle X-rays were recorded (Fig. 4) and the intensity changes of one myosin meridional reflection (1st MM) and two actin-layer lines (6th and 7th ALLs) were monitored and analyzed (Fig. 5). All these parameters were enhanced on addition of Ca²⁺ in WT as well as in *Myh4^{ar1}/+* mice. Of particular interest, during activation, the 1st MM was significantly greater in *Myh4^{ar1}/+* when compared with WT mice (Fig. 5). The 6th and 7th ALLs, by contrast, were not affected by the presence of the mutation (Fig. 5).

As for equatorial reflections (Fig. 6), the I_{1,1}/I_{1,0} intensity ratios were calculated and gave information on the mass distribution between the thick and thin filaments. Under resting conditions, the I_{1,1}/I_{1,0} intensity ratio was not different between *Myh4^{ar1}/+* and WT mice (Fig. 5). Upon activation, this ratio was significantly greater in *Myh4^{ar1}/+* when compared with WT mice (Fig. 5). The I_{1,0} equatorial reflections were also converted to d_{1,0} lattice spacings, using Bragg's Law (Colson et al., 2007). This value is known to reflect the radial compressional forces. Under resting conditions and during contraction, d_{1,0} lattice spacings were not different between *Myh4^{ar1}/+* and WT mice (Fig. 5). The widths of the I_{1,0} equatorial reflections (estimated via $\Delta_{1,0}$) were also similar between *Myh4^{ar1}/+* and WT mice under resting conditions (Fig. 5), but were significantly greater, upon activation, in *Myh4^{ar1}/+* when compared with WT mice (Fig. 5).

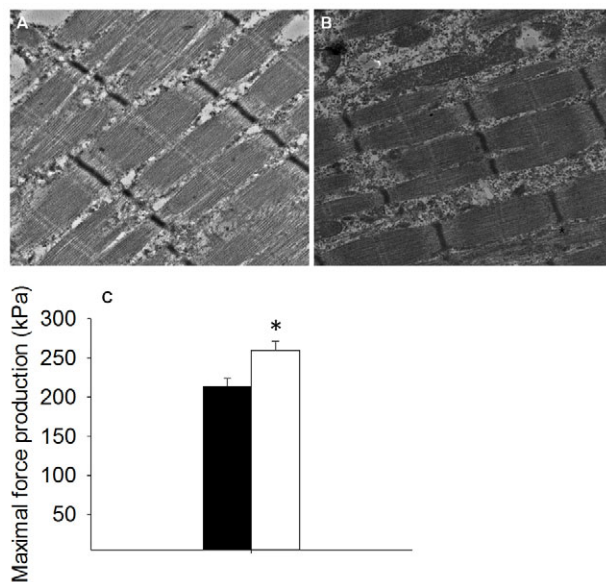


Fig. 1. Preserved muscle ultrastructure and increased force production in *Myh4^{ar1}/+* mice. This figure depicts typical electron microscopy pictures for WT (A) and for *Myh4^{ar1}/+* (B) mice, as well as the maximal steady-state isometric force production of membrane-permeabilized single fibers (C) for WT (black bar) and *Myh4^{ar1}/+* (white bar). Asterisks denote significant differences ($P < 0.05$) when compared with WT.

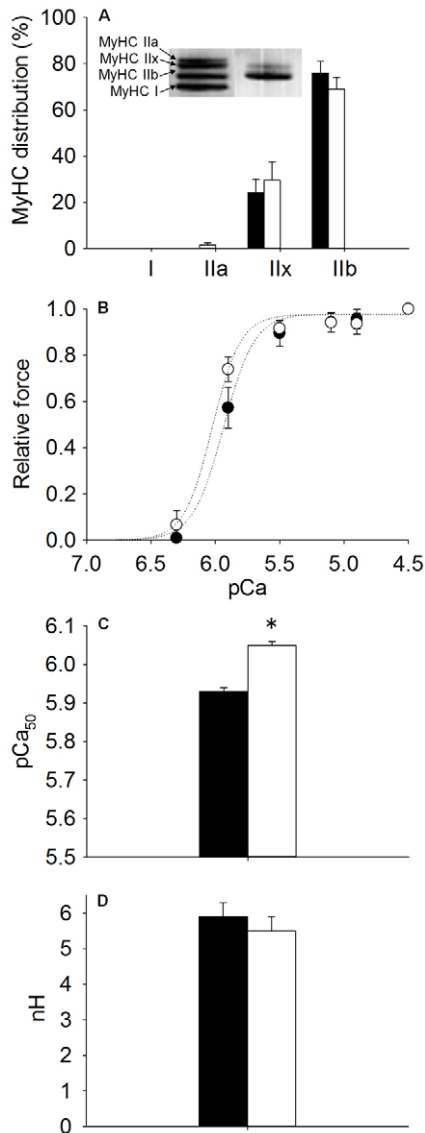


Fig. 2. Increased fiber Ca^{2+} sensitivity of force in *Myh4^{arl/+}* mice. This figure displays the MyHC isoform distribution in EDL for WT (black) and *Myh4^{arl/+}* (white) (A) fibers, as well as the relative force-pCa relationships (B), Ca^{2+} sensitivity of force (pCa_{50}) (C) and Hill coefficient (nH) (D). Values are shown as means and standard errors. Asterisks denote significant differences ($P < 0.05$) when compared with WT.

DISCUSSION

Understanding the molecular functional effects of mutants in myosinopathies is crucial to establish potential therapeutic strategies. In the present study, we proved that, in the presence of MYH4^{L342Q}, the strong binding of myosin heads to actin filaments is greatly modified during contraction, triggering an increase in force production and, ultimately, probably disrupting muscle structure when the number of mutated molecules is high.

Altered myosin binding to actin filaments

As shown in Fig. 1, the steady-state isometric maximal force of single membrane-permeabilized muscle fibers from heterozygous

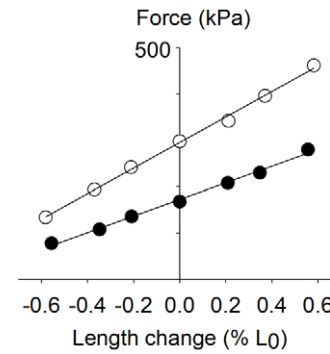


Fig. 3. Enhanced fiber stiffness in *Myh4^{arl/+}* mice. This figure shows typical peak force-length change relationships for WT (black circles) and *Myh4^{arl/+}* (white circles).

mice (*Myh4^{arl/+}*) was greater when compared with WT cells. This can be due to either a higher number of strongly attached myosin cross-bridges and/or to a larger force per individual actomyosin interaction. To distinguish between these two alternatives, stiffness measurements were achieved. Active stiffness was higher in *Myh4^{arl/+}* when compared with WT fibers, whereas rigor stiffness was unchanged. This implies that the higher force in the presence of the mutation is mainly caused by an increase in the proportion of myosin heads that are strongly bound to actin filaments rather than a change in the force developed by individual cross-bridges. What are the underlying mechanisms? The fraction of strongly bound myosin cross-bridges depends on $f_{app}/(f_{app} + g_{app})$ (Brenner and Eisenberg, 1986; Huxley, 1957), with f_{app} being the rate constant for attachment and g_{app} the rate constant for detachment (Brenner, 1988). We can therefore hypothesize that, in the presence of the MYH4^{L342Q} defect, either an increase in f_{app} and/or a decrease in g_{app} occurs. Because the rate of force redevelopment, k_{tr} , was unchanged in *Myh4^{arl/+}* animals when compared with WT mice (Kurapati et al., 2012) and because k_{tr} is proportional to $f_{app} + g_{app}$ (Brenner and Eisenberg, 1986; Huxley, 1957), we suggest a direct effect on both f_{app} and g_{app} (faster f_{app} and slower g_{app}). Thus, one can postulate that the cross-bridge cycling kinetics is modified in *Myh4^{arl/+}* mice, inducing an increased time spent by individual myosin heads in a strongly bound force-generating state, and thus conducting to an increased proportion of strongly bound myosin cross-bridges.

X-ray data seemed to confirm the above findings. In the present study, the 1st MM and 6th and 7th ALLs were analyzed. The 1st MM (meridional reflection at 14.5 nm) is thought to reflect the average orientation of the myosin cross-bridges with respect to the thick-filament backbone (Huxley et al., 1983; Reconditi et al., 2005). Indeed, its intensity is weak when myosin heads are at oblique angles or have a wide range of axial angles. It becomes stronger when myosin cross-bridges are more perpendicular to the thick-

Table 1. Single muscle fiber mechanics

	<i>Myh4^{arl/+}</i>	WT
Active stiffness ($\text{kPa} \cdot \% L_0^{-1}$)	151.90 ± 11.60* (n=17)	120.80 ± 13.90 (n=12)
Rigor stiffness ($\text{kPa} \cdot \% L_0^{-1}$)	214.00 ± 21.90 (n=17)	211.10 ± 16.60 (n=12)

* indicates a significant difference when compared with WT ($P < 0.05$). For each parameter, n represents the number of tested fibers.

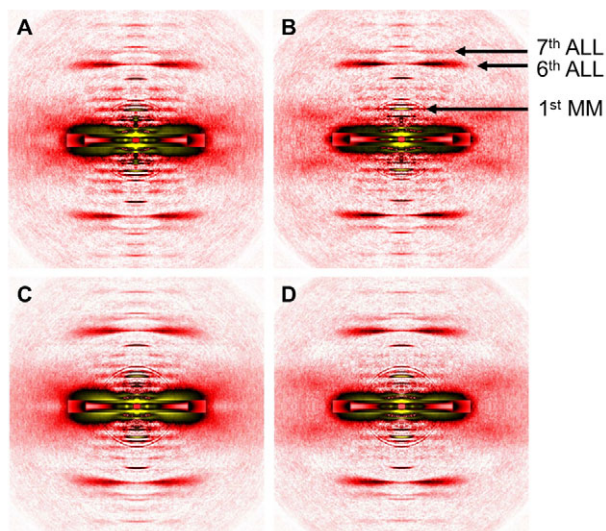


Fig. 4. Typical low-angle X-ray diffraction reflection patterns. This figure shows diffraction patterns for WT (A,B) or *Myh4^{arl/+}* (C,D) mice in resting state (A,C) or upon activation (B,D).

filament axis, as is the case during contraction (Huxley et al., 1983; Reconditi et al., 2005). The 6th and 7th ALLs (actin-layer lines at 5.9 and 5.1 nm, respectively) are likely to provide information about actin monomers modifying their molecular shape (Yagi and Matsubara, 1988). In the present study, because the 6th and 7th ALLs were not different between WT and *Myh4^{arl/+}* mice, one can propose that the mutation does not affect actin conformational changes. By contrast, because the 1st MM was enhanced in the presence of MYH4^{L342Q}, we suggest that the mean orientation of the myosin heads that are strongly bound to actin monomers is more perpendicular than those that are weakly bound. One reasonable explanation for this phenomenon is that the greater fraction of strongly bound cross-bridges is caused by fine tunings of f_{app} and g_{app} changing transitions (i) from the weak to the strong force-producing binding state; and (ii) from the strong to the weak state. In the present study, unfortunately, direct quantifications of f_{app} and g_{app} have not been performed but could constitute the main objective of one future study.

What are the potential causes of f_{app} and g_{app} modifications? L342 is a highly conserved amino acid located in the catalytic domain of the myosin molecule and very close to sites involved in ATP and ADP exchanges (Rayment et al., 1993a; Rayment et al., 1993b; Rayment et al., 1996). Consequently, the replacement of a leucine by a glutamine at position 342 might directly prevent proper ATP binding and/or ADP dissociation. In addition to this, the mutation could have other consequences. Indeed, as presented in Fig. 2, the effect on force production is exacerbated at submaximal $[Ca^{2+}]$. The exact underlying mechanisms remain unclear, but a recent simple analytical model predicts that changes in f_{app} and g_{app} are likely to affect the Ca^{2+} sensitivity of force production (Sich et al., 2010). Other unknown phenomena might also occur. Further experiments are required to specifically study this aspect.

The analysis of the equatorial reflections also validates the mechanical results (Fig. 5). Indeed, the $I_{1,1}/I_{1,0}$ intensity ratio was much more increased during contraction in *Myh4^{arl/+}* mice when

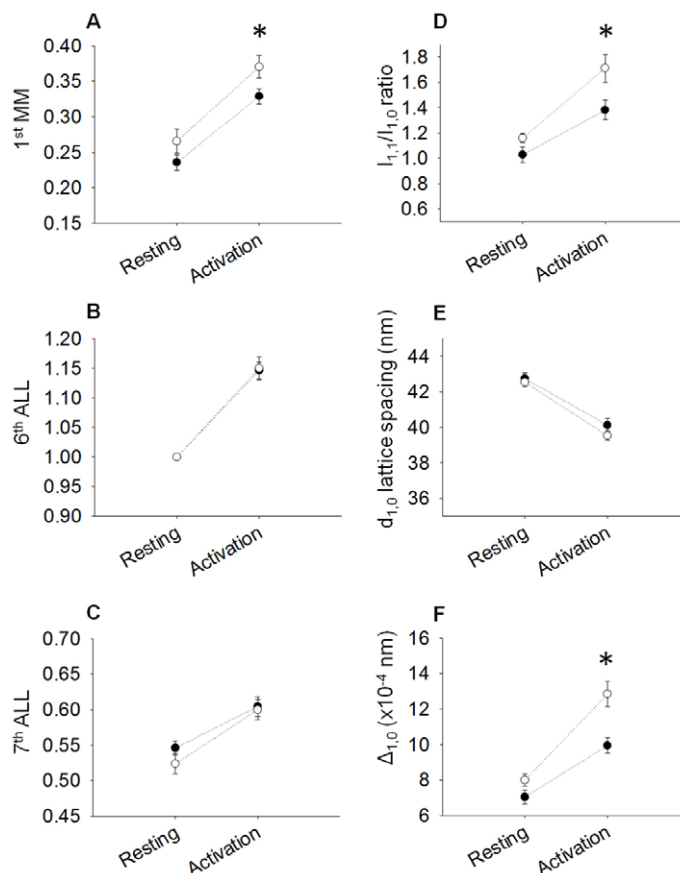


Fig. 5. Changes in low-angle X-ray diffraction reflections in *Myh4^{arl/+}* mice. Meridional (A), actin-layer lines (ALLs; B,C) and equatorial (D-F) reflections are presented. Values are shown as means and standard errors for WT ($n=23$; black circles) and *Myh4^{arl/+}* ($n=21$; white circles) mice. Asterisks denote significant differences ($P < 0.05$) when compared with WT.

compared with WT rodents, indicating a more pronounced net transfer of mass from the thick to thin filaments, thus a greater number of myosin cross-bridges bound to actin monomers. In addition, interestingly, the widths of the equatorial reflections were larger in *Myh4^{arl/+}* when compared with WT mice (Fig. 5), reflecting a higher degree of variance in lattice spacing inhomogeneity. One plausible explanation is that the myofilaments are displaced from their equilibrium positions in the presence of the MYH4^{L342Q} mutation, leading to a greater disorder of the hexagonal myofilament lattice under activating conditions.

When all the above findings are taken together, it seems that, in the presence of MYH4^{L342Q}, the amount of strongly bound myosin cross-bridges is increased by ~20-25% (Table 1, Fig. 5). However, in *Myh4^{arl/+}* animals, the mutant peptide is present at only 7% of

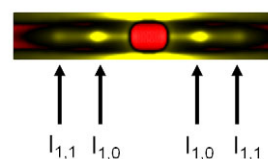


Fig. 6. Typical equatorial reflection for WT mice.

the WT protein levels (Kurapati et al., 2012). From where does the discrepancy arise? It remains unknown. Nevertheless, as previously reported with a mutation in myosin light chain (Kazmierczak et al., 2012), mutant proteins expressed at very low levels (below 10%) might function as poison peptides that also alter the function of the normal proteins, leading to an overall myosin dysfunction (>20%).

Comparison with other MyHC mutations

A few other mutations located in the catalytic domain have been functionally studied and findings were analogous. For instance, MYH7^{R403Q} and MYH7^{R403W}, which lie in the actin-binding interface, do not alter the force per individual actomyosin interaction (keeping the myosin tilting to ~7 nm) but prolong the time spent by each myosin molecule in the strong binding conformation (Palmiter et al., 2000) and promoting force generation (Belus et al., 2008; Debold et al., 2007; Keller et al., 2004). Similarly, the MYH7^{R453C} mutation, located close to the nucleotide-binding pocket (Oldfors, 2007; Rayment et al., 1995), seems to allow myosin molecules to spend a greater fraction of the cross-bridge cycle strongly bound to actin filament, increasing the duty ratio and enhancing force production (Debold et al., 2007; Wang et al., 2003). Another mutation, MYH7^{R719W}, close to the catalytic domain but located in the converter region, has been shown to increase the stiffness of individual myosin heads, leading to an increased resistance to elastic distortion and enhanced force production (Seeböhm et al., 2009).

Conclusion

Taken together, the present data suggest that, in the presence of the MYH4^{L342Q} mutation, many important dysfunctional processes happen. Myosin binding to actin monomers is favored, increasing the amount of strongly bound myosin cross-bridges. At the cellular level, this increases the steady-state isometric force production and helps explain why higher levels of MYH4^{L342Q} in homozygous mice triggers hind-limb muscle paralysis and myofibrillar disorganization. Overall, all this has to be considered when designing future drug therapies for myosinopathies.

MATERIALS AND METHODS

Animals

Two- to three-month-old WT mice as well as age-matched heterozygous transgenic animals expressing MYH4^{L342Q} (*Myh4^{lar1/+}*) were included in the analyses. A complete description of the mice can be found elsewhere (Kurapati et al., 2012). Mice were killed by cervical dislocation and skeletal muscles [tibialis anterior and extensor digitorum longus (EDL)] were dissected. All procedures involving animal care and handling were performed according to institutional guidelines and were reviewed and approved by the Uppsala Local Ethical Committee on Animal Research.

Muscle preparation

Specimens were placed in relaxing solution at 4°C. Bundles of ~50 fibers were dissected free and then tied with surgical silk to glass capillary tubes at slightly stretched lengths. They were then treated with skinning solution (relaxing solution containing glycerol; 50:50 v/v) for 24 hours at 4°C, after which they were transferred to -20°C.

In addition, the muscle bundles were treated with sucrose, a cryoprotectant, within 1-2 weeks for long-term storage (Frontera and Larsson, 1997). They were detached from the capillary tubes and snap frozen in liquid-nitrogen-chilled propane and stored at -160°C.

Membrane-permeabilized fiber mechanical recordings and analyses

On the day of experiment, bundles were de-sucrosed, transferred to a relaxing solution and single fibers dissected. A fiber 1-2 mm long was left between connectors leading to a force transducer (model 400A, Aurora Scientific) and a lever arm system (model 308B, Aurora Scientific) (Larsson and Moss, 1993; Moss, 1979). The two extremities of the fiber were tightly attached to the connectors as previously described (Moss, 1979). The apparatus was mounted on the stage of an inverted microscope (model IX70; Olympus). The sarcomere length was set to 2.50-2.60 μm (optimal mouse sarcomere length where the force production is the highest) and controlled during the experiment using a high-speed video analysis system (model 901A HVSL, Aurora Scientific). The diameter of the fiber between the connectors was measured through the microscope at a magnification of 320 \times with an image analysis system prior to the mechanical experiments. Fiber depth was measured by recording the vertical displacement of the microscope nosepiece while focusing on the top and bottom surfaces of the fiber. The focusing control of the microscope was used as a micrometer. Cross-sectional area (CSA) was calculated from the diameter and depth, assuming an elliptical circumference, and was corrected for the 20% swelling that is known to occur during skinning (Moss, 1979). Diameter and depth were measured at three different locations along the length of each fiber and the mean was considered as representative of cell dimensions. Mechanical experiments were performed at 15°C and included force measurements (normalized to CSA) after various length steps at numerous $[\text{Ca}^{2+}]$ (pCas between 6.30 and 4.50), as previously described (Ochala et al., 2011; Ochala et al., 2008; Ochala et al., 2007).

For the mechanical recordings, relaxing and activating solutions contained (in mM) 4 Mg-ATP, 1 free Mg^{2+} , 20 imidazole, 7 EGTA, 14.5 creatine phosphate, and KCl to adjust the ionic strength to 180 mM and pH to 7.0. The pre-activating solution was identical to the relaxing solution except that the EGTA concentration was reduced to 0.5 mM. The concentrations of free Ca^{2+} were 10^{-9} M (relaxing and pre-activating solutions) and $10^{-6.30}$, $10^{-5.90}$, $10^{-5.50}$, $10^{-5.10}$, $10^{-4.90}$ and $10^{-4.50}$ M (activating solutions), expressed as pCas (i.e. $-\log_{10} [\text{Ca}^{2+}]$). The rigor solution was the same as the regular activating solution except that MgATP and creatine phosphate were absent.

After mechanical recordings, each skinned fiber was placed in urea buffer (120 g urea, 38 g thiourea, 70 ml H_2O , 25 g mixed bed resin, 2.89 g dithiothreitol, 1.51 g Trizma base, 7.5 g SDS, 0.004% bromophenol blue) in a plastic microcentrifuge tube and stored at -160°C. MyHC isoform composition of fibers was then determined by 6% SDS-PAGE. The acrylamide concentration was 4% (wt/vol) in the stacking gel and 6% in the running gel, and the gel matrix included 30% glycerol. Sample loads were kept small (equivalent to ~0.05 mm of fiber segment) to improve the resolution of the myosin heavy chain bands (types I, IIa, IIx and IIb). Electrophoresis

was performed at 120 V for 24 hour with a Tris-glycine electrode buffer (pH 8.3) at 15°C (SE 600 vertical slab gel unit, Hoefer Scientific Instruments). The gels were silver-stained and subsequently scanned in a soft laser densitometer (Molecular Dynamics) with a high spatial resolution (50 µm pixel spacing) and 4096 optical density levels.

X-ray diffraction recordings and analyses

Two to three days prior to X-ray recordings, bundles were desucrosed, transferred to a relaxing solution and single fibers were dissected. Arrays of ~30 fibers were set up (Iwamoto, 2009; Iwamoto et al., 2001; Iwamoto et al., 2002; Iwamoto et al., 2003; Ochala et al., 2011; Ochala et al., 2010). For each fiber, both ends were clamped to half-split gold meshes for electron microscopy (width, 3 mm), which had been glued to precision-machined ceramic chips (width, 3 mm) designed to fit to a specimen chamber. The arrays were then transferred to the skinning solution and stored at -20°C. 44 arrays were mounted.

On the day of X-ray recordings, arrays were placed in a plastic dish containing a pre-activating solution and washed thoroughly to remove the glycerol. They were then transferred to the specimen chamber, capable of manual length adjustment and force measurement (force transducer, AE801, Memscap, Bernin, France), filled with a pre-activating solution. Mean sarcomere length was measured and set to 2.50 µm. Subsequently, X-ray diffraction patterns were recorded at 15°C, first in the pre-activating solution and then in the activating solution (pCa 4.50) when maximal steady-state isometric force was reached. It should be mentioned that the activating solution was supplied to the chamber by a remote-controlled pump.

For each array, ~10-20 diffraction patterns were recorded for each solution at the BL45XU beamline of SPring-8 and were analyzed as described previously (Iwamoto, 2009; Iwamoto et al., 2001; Iwamoto et al., 2002; Iwamoto et al., 2003). The wavelength was 0.09 nm and the specimen-to-detector distance was 2 m. As a detector, a cooled CCD camera (C4880, Hamamatsu Photonics; 1000×1018 pixels) was used in combination with an image intensifier (VP5445, Hamamatsu Photonics). To minimize radiation damages, the exposure time was kept low (2 seconds) and the specimen chamber was moved by 100 µm after each exposure. Moreover, we placed an aluminum plate (thickness, 0.35-0.5 mm) upstream of the specimen chamber. The beam flux was estimated to be between 2.7×10^{11} and 4.0×10^{11} photons/second after attenuation, and the beam size at the sample position was 0.2 mm (vertical) and 0.3 mm (horizontal). Following X-ray recordings, background scattering was subtracted, and reflection intensities (except for equatorial reflections) were determined as described elsewhere (Iwamoto, 2009; Iwamoto et al., 2001; Iwamoto et al., 2002; Iwamoto et al., 2003; Yagi, 2003). The intensities of equatorial reflections were determined separately. First, the background (the region outside the area of 1,0 and 1,1 reflections) was approximated by a single exponential decay function, and this was subtracted from the observed intensity profile. The resulting curve should contain the profiles of 1,0, 1,1 and 2,0 reflections of the hexagonal lattice of myofibrils, and the profile of the square lattice of Z-line components. In this curve, the 1,0 is usually the most prominent reflection, and this was first fitted by a Gaussian distribution function and was subtracted from the rest of the curve. After this,

the 1,1 is the most prominent reflection, and this was again fitted by a Gaussian. The intensities of 1,0 and 1,1 were defined as the areas below the fitted Gaussian curves. The lattice spacing was calculated from the peak position of the Gaussian curve.

Statistical analyses

Data are presented as means ± s.e.m. Sigma Stat software (Jandel Scientific) was used to generate descriptive statistics. The unpaired Student's *t*-test was applied, and in cases where the data did not meet the criteria of normality (Kolmogorov-Smirnov test, $P < 0.05$), the non-parametric Mann-Whitney rank-sum test was performed. Otherwise, regressions were performed and relationships were considered significantly different from zero at $P < 0.05$.

ACKNOWLEDGEMENTS

We are grateful to Prof. L. Larsson for making the mechanical experiments possible. We also thank Y. Hedström and A. M. Gustafson for excellent technical assistance. The X-ray experiments were performed under approval of the SPring-8 Proposal Review Committee (2011A1042).

COMPETING INTERESTS

The authors declare that they do not have any competing or financial interests.

AUTHOR CONTRIBUTIONS

H.I., G.B. and J.O. conceived and designed the experiments. J.L., H.I., G.B. and J.O. performed the experiments. J.L., H.I. and J.O. analyzed the data. J.L., H.I., G.B. and J.O. wrote the paper.

FUNDING

This study was supported by grants from STINT, from the Swedish Research Council and Harald och Greta Jeansson's Stiftelse to J.O., and from the UK Medical Research Council and the Biology Department, University of York, UK to G.B.

REFERENCES

- Belus, A., Piroddi, N., Scellini, B., Tesi, C., Amati, G. D., Girolami, F., Yacoub, M., Cecchi, F., Olivetto, I. and Poggesi, C. (2008). The familial hypertrophic cardiomyopathy-associated myosin mutation R403Q accelerates tension generation and relaxation of human cardiac myofibrils. *J. Physiol.* **586**, 3639-3644.
- Brenner, B. (1988). Effect of Ca²⁺ on cross-bridge turnover kinetics in skinned single rabbit psoas fibers: implications for regulation of muscle contraction. *Proc. Natl. Acad. Sci. USA* **85**, 3265-3269.
- Brenner, B. and Eisenberg, E. (1986). Rate of force generation in muscle: correlation with actomyosin ATPase activity in solution. *Proc. Natl. Acad. Sci. USA* **83**, 3542-3546.
- Colson, B. A., Bekyarova, T., Fitzsimons, D. P., Irving, T. C. and Moss, R. L. (2007). Radial displacement of myosin cross-bridges in mouse myocardium due to ablation of myosin binding protein-C. *J. Mol. Biol.* **367**, 36-41.
- Cooke, R. and Franks, K. (1980). All myosin heads form bonds with actin in rigor rabbit skeletal muscle. *Biochemistry* **19**, 2265-2269.
- Debold, E. P., Schmitt, J. P., Patlak, J. B., Beck, S. E., Moore, J. R., Seidman, J. G., Seidman, C. and Warshaw, D. M. (2007). Hypertrophic and dilated cardiomyopathy mutations differentially affect the molecular force generation of mouse alpha-cardiac myosin in the laser trap assay. *Am. J. Physiol.* **293**, H284-H291.
- Frontera, W. R. and Larsson, L. (1997). Contractile studies of single human skeletal muscle fibers: a comparison of different muscles, permeabilization procedures, and storage techniques. *Muscle Nerve* **20**, 948-952.
- Huxley, A. F. (1957). Muscle structure and theories of contraction. *Prog. Biophys.* **7**, 255-318.
- Huxley, H. E., Simmons, R. M., Faruqi, A. R., Kress, M., Bordas, J. and Koch, M. H. (1983). Changes in the X-ray reflections from contracting muscle during rapid mechanical transients and their structural implications. *J. Mol. Biol.* **169**, 469-506.
- Iwamoto, H. (2009). Evidence for unique structural change of thin filaments upon calcium activation of insect flight muscle. *J. Mol. Biol.* **390**, 99-111.
- Iwamoto, H., Oiwa, K., Suzuki, T. and Fujisawa, T. (2001). X-ray diffraction evidence for the lack of stereospecific protein interactions in highly activated actomyosin complex. *J. Mol. Biol.* **305**, 863-874.
- Iwamoto, H., Oiwa, K., Suzuki, T. and Fujisawa, T. (2002). States of thin filament regulatory proteins as revealed by combined cross-linking/X-ray diffraction techniques. *J. Mol. Biol.* **317**, 707-720.
- Iwamoto, H., Wakayama, J., Fujisawa, T. and Yagi, N. (2003). Static and dynamic x-ray diffraction recordings from living mammalian and amphibian skeletal muscles. *Biophys. J.* **85**, 2492-2506.

- Kazmierczak, K., Muthu, P., Huang, W., Jones, M., Wang, Y. and Szczesna-Cordary, D.** (2012). Myosin regulatory light chain mutation found in hypertrophic cardiomyopathy patients increases isometric force production in transgenic mice. *Biochem. J.* **442**, 95-103.
- Keller, D. I., Coirault, C., Rau, T., Cheav, T., Weyand, M., Amann, K., Lecarpentier, Y., Richard, P., Eschenhagen, T. and Carrier, L.** (2004). Human homozygous R403W mutant cardiac myosin presents disproportionate enhancement of mechanical and enzymatic properties. *J. Mol. Cell. Cardiol.* **36**, 355-362.
- Kurapati, R., McKenna, C., Lindqvist, J., Williams, D., Simon, M., LeProust, E., Baker, J., Cheeseman, M., Carroll, N., Denny, P. et al.** (2012). Myofibrillar myopathy caused by a mutation in the motor domain of mouse MyHC IIb. *Hum. Mol. Genet.* **21**, 1706-1724.
- Larsson, L. and Moss, R. L.** (1993). Maximum velocity of shortening in relation to myosin isoform composition in single fibres from human skeletal muscles. *J. Physiol.* **472**, 595-614.
- Moss, R. L.** (1979). Sarcomere length-tension relations of frog skinned muscle fibres during calcium activation at short lengths. *J. Physiol.* **292**, 177-192.
- Ochala, J., Li, M., Tajsharghi, H., Kimber, E., Tulinus, M., Oldfors, A. and Larsson, L.** (2007). Effects of a R133W beta-tropomyosin mutation on regulation of muscle contraction in single human muscle fibres. *J. Physiol.* **581**, 1283-1292.
- Ochala, J., Li, M., Ohlsson, M., Oldfors, A. and Larsson, L.** (2008). Defective regulation of contractile function in muscle fibres carrying an E41K beta-tropomyosin mutation. *J. Physiol.* **586**, 2993-3004.
- Ochala, J., Iwamoto, H., Larsson, L. and Yagi, N.** (2010). A myopathy-linked tropomyosin mutation severely alters thin filament conformational changes during activation. *Proc. Natl. Acad. Sci. USA* **107**, 9807-9812.
- Ochala, J., Lehtokari, V. L., Iwamoto, H., Li, M., Feng, H. Z., Jin, J. P., Yagi, N., Wallgren-Pettersson, C., Pénisson-Besnier, I. and Larsson, L.** (2011). Disrupted myosin cross-bridge cycling kinetics triggers muscle weakness in nebulin-related myopathy. *FASEB J.* **25**, 1903-1913.
- Oldfors, A.** (2007). Hereditary myosin myopathies. *Neuromuscul. Disord.* **17**, 355-367.
- Palmiter, K. A., Tyska, M. J., Haeberle, J. R., Alpert, N. R., Fananapazir, L. and Warshaw, D. M.** (2000). R403Q and L908V mutant beta-cardiac myosin from patients with familial hypertrophic cardiomyopathy exhibit enhanced mechanical performance at the single molecule level. *J. Muscle Res. Cell Motil.* **21**, 609-620.
- Rayment, I., Holden, H. M., Whittaker, M., Yohn, C. B., Lorenz, M., Holmes, K. C. and Milligan, R. A.** (1993a). Structure of the actin-myosin complex and its implications for muscle contraction. *Science* **261**, 58-65.
- Rayment, I., Rypniewski, W. R., Schmidt-Bäse, K., Smith, R., Tomchick, D. R., Benning, M. M., Winkelmann, D. A., Wesenberg, G. and Holden, H. M.** (1993b). Three-dimensional structure of myosin subfragment-1: a molecular motor. *Science* **261**, 50-58.
- Rayment, I., Holden, H. M., Sellers, J. R., Fananapazir, L. and Epstein, N. D.** (1995). Structural interpretation of the mutations in the beta-cardiac myosin that have been implicated in familial hypertrophic cardiomyopathy. *Proc. Natl. Acad. Sci. USA* **92**, 3864-3868.
- Rayment, I., Smith, C. and Yount, R. G.** (1996). The active site of myosin. *Annu. Rev. Physiol.* **58**, 671-702.
- Reconditi, M., Linari, M., Lucii, L., Stewart, A., Sun, Y. B., Narayanan, T., Irving, T., Piazzesi, G., Irving, M. and Lombardi, V.** (2005). Structure-function relation of the myosin motor in striated muscle. *Ann. N. Y. Acad. Sci.* **1047**, 232-247.
- Seebohm, B., Matinmehr, F., Köhler, J., Francino, A., Navarro-López, F., Perrot, A., Ozelik, C., McKenna, W. J., Brenner, B. and Kraft, T.** (2009). Cardiomyopathy mutations reveal variable region of myosin converter as major element of cross-bridge compliance. *Biophys. J.* **97**, 806-824.
- Sich, N. M., O'Donnell, T. J., Coulter, S. A., John, O. A., Carter, M. S., Cremo, C. R. and Baker, J. E.** (2010). Effects of actin-myosin kinetics on the calcium sensitivity of regulated thin filaments. *J. Biol. Chem.* **285**, 39150-39159.
- Wang, Q., Moncman, C. L. and Winkelmann, D. A.** (2003). Mutations in the motor domain modulate myosin activity and myofibril organization. *J. Cell Sci.* **116**, 4227-4238.
- Yagi, N.** (2003). An x-ray diffraction study on early structural changes in skeletal muscle contraction. *Biophys. J.* **84**, 1093-1102.
- Yagi, N. and Matsubara, I.** (1988). Changes in the 5.9 nm actin layer-line on activation of frog skeletal muscles. *Adv. Exp. Med. Biol.* **226**, 369-380.